Coherent Vibrational Motion during the Excited-State Intramolecular Proton Transfer Reaction in *o*-Hydroxyacetophenone

Charlene Su, Jui-Ying Lin, Re-Ming R. Hsieh, and Po-Yuan Cheng*

Department of Chemistry, National Tsing Hua University, Hsinchu, Taiwan, R.O.C.

Received: September 8, 2002

Excited-state intramolecular proton transfer (ESIPT) reaction dynamics in *o*-hydroxyacetophenone (OHAP) has been investigated in a supersonic molecular beam using femtosecond time-resolved multiphoton ionization mass spectrometry. The observed transients exhibit a biexponential decay and a rapidly damped oscillation with a period of ∼600 fs. The combinations of experimental and theoretical results suggested that the oscillation is due to a coherent vibrational motion that follows the molecular transformation from the initial enol configuration to the final keto form during the ESIPT reaction.

I. Introduction

When a molecule is excited with an ultrafast laser pulse, an initially localized nuclear wave packet can be prepared via coherent excitation of several vibrational eigenstates. The time evolution of the wave packet on the global potential energy surface (PES) is governed by the system's molecular Hamiltonian and reflects the underlying dynamics, either reactive or nonreactive. Zewail's group[1] was the first to demonstrate this concept in simple systems of NaI[2] and I_2.[3] For simple reactive systems, wave packet motion along and/or perpendicular to the reaction coordinate can reveal important transition-state resonance structures.[4] However, in large complex systems the interpretations are sometimes ambiguous, because coherent motions can also occur in modes not strongly coupled to the reaction coordinate and are therefore not directly relevant to the reaction dynamics. In this Letter, we report an unambiguous observation of a coherent nuclear wave packet motion during the excited-state intramolecular proton transfer (ESIPT) reaction in a complex system under isolated conditions.

ESIPT usually occurs in molecules having an intramolecular hydrogen bond between two electronegative heteroatoms, A−H···B, which usually forms a chelate ring. Upon photoexcitation the molecule evolves to a distinct excited-state equilibrium configuration, A···H−B, by shifting the partially charged hydrogen atom (or the proton).[5−7] The substantial structural change is manifested by the largely red-shifted fluorescence generally observed in this type of molecules.[5−7] The system of interest here is *o*-hydroxyacetophenone (OHAP). It and its close analogue, *o*-hydroxybenzaldehyde (OHBA), are among the simplest aromatic molecules exhibiting ESIPT. The molecular structures of its two tautomeric forms are illustrated in Figure 1. The first absorption band of OHAP centers at ∼320 nm[8−10] and has been shown to be primarily due to the lowest π,π^* excitation.[10,11] OHAP exhibits a very large fluorescence red shift of more than 10 000 cm^{-1} upon excitation to this band in both liquid[9] and vapor phases,[8] suggesting the occurrence of ESIPT. Because no mirror-image emission has been observed, it was proposed that the reaction occurs in an ultrafast time scale.[9,10] Zewail's group studied the ESIPT reaction in methyl salicylate (MS), a close analogue to OHAP, in the bulk vapor phase and concluded that the reaction occurs in less than 60 fs.[12] Recently, Stolow's group studied the ESIPT reaction in OHBA using femtosecond (fs) time-resolved photoelectron spectroscopy in a molecular beam.[13] They also concluded that the reaction occurs in less than 50 fs. Ab initio calculations at

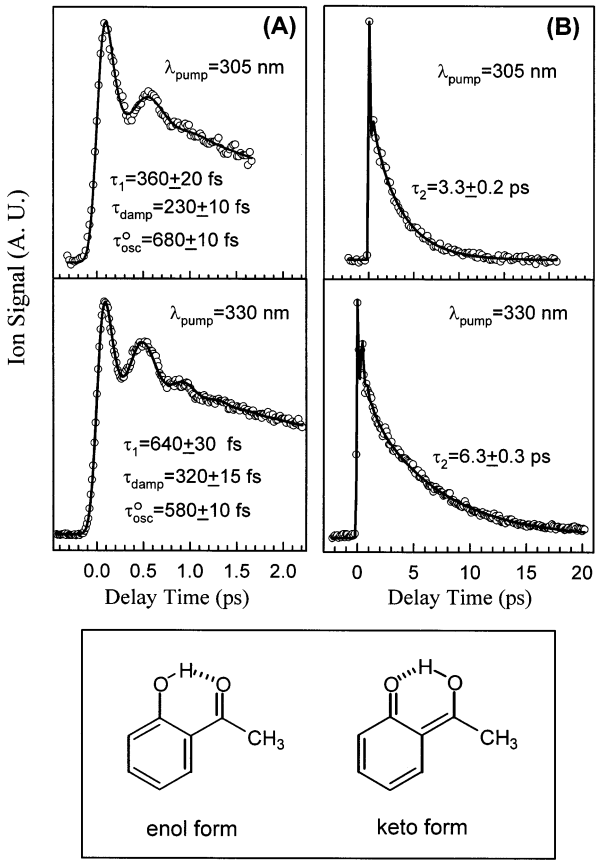

Figure 1. Upper: short-time scale (A) and long-time scale (B) OHAP transients obtained with 330 and 305 nm excitations. The circles are experimental data, and the solid lines are the best fits to the model function eq 1 convoluted with the response function, as described in the text. The parameters obtained from the fits are indicated in the figure. Lower: molecular structures of OHAP in the enol and keto forms.

* Corresponding author. E-mail: pycheng@mx.nthu.edu.tw. Fax: 886-3-571-1082.

10.1021/jp026944n CCC: $22.00
Published on Web 11/23/2002

various levels of theory have shown that the ESIPT reactions in OHBA[10,14,15] and OHAP[16] involve an asymmetric single-minimum potential-energy (PE) profile with no barrier between the enol and keto forms, consistent with the above experimental conclusions. The energy difference between the vertically excited enol configuration and the equilibrium keto configuration in the OHBA first singlet (π,π^*) state has been predicted to be about 0.5 eV (CASPT2) or 0.3 eV (TDDFT).[15]

In our studies the ESIPT dynamics in OHAP was investigated using femtosecond time-resolved mulitiphoton ionization mass spectrometry in a molecular beam. The technique measures the time-dependent multiphoton ionization yield of the excited state as it evolves in time after the initial excitation.[1] We observed, in addition to the expected ultrafast decays, a rapidly damped oscillatory component that can be attributed to a coherent vibrational motion in the system. Although similar observations have been reported previously for larger ESIPT molecular systems in liquid solutions,[17,18] this is the first time such a behavior has ever been observed under isolated conditions in a molecular beam.

II. Experimental Section

The femtosecond laser system employed in this work consisted of a self-mode-locked Ti:sapphire laser, a 1 kHz chirp-pulse regenerative amplifier (CPA), and an optical parametric amplifier. The CPA output was split into two parts by a beam splitter. The major portion (~80%) of the beam was used to pump the OPA, and its output was subsequently frequency doubled twice by two thin BBO crystals and recompressed by a prism pair. The resultant tunable femtosecond pulses in the UV region from 305 to 340 nm were used as the pump. The remaining portion of the CPA output (~20%) was directed through a computer-controlled optical delay line and was used as the probe. A polarizer was placed in the probe beam path to set its polarization at the magic angle (54.7°) with respect to that of the pump to minimize the rotational coherence effect.[19] The pump and probe beams were then collinearly recombined via a dichroic mirror and focused through a $f = 500$ mm lens into the extraction region of a homemade time-of-flight mass spectrometer (TOF-MS) housed in a conventional two-chamber molecular beam apparatus. The pulse energies were attenuated to ~0.1 μJ for the pump and ~10 μJ for the probe before entering the window. OHAP vapor at room temperature was coexpanded with ~1 atm He gas through a 75 μm pinhole to form a continuous supersonic jet in the first chamber. The jet was skimmed before entering the second chamber where it was intersected by the femtosecond laser pulses in the extraction region of the TOF-MS. The transients were obtained by monitoring the ion signal at the parent ion mass channel while the pump vs probe delay time was scanned.

III. Results and Discussion

Figure 1 shows the OHAP transients obtained at two representative excitation wavelengths, 330 and 305 nm. The former corresponds to the excitation near the peak of the first absorption band, whereas the latter excites at the blue tail. In general, a rapidly damped oscillation with a period of ~600 fs was clearly observed within the first picosecond. In longer time scales the transients decay with time constants of several picosecond (Figure 1B). Careful investigations on the laser irradiance dependence suggested that the transient signal is due to absorption of one pump photon and three to four probe photons. For the transients shown in Figure 1, the pump and probe pulse energies were kept at the lowest level possible to avoid interference from saturation and higher order multiphoton excitation. Excitation at other wavelengths within the first absorption band of OHAP between 305 and 340 nm resulted in similar transients.

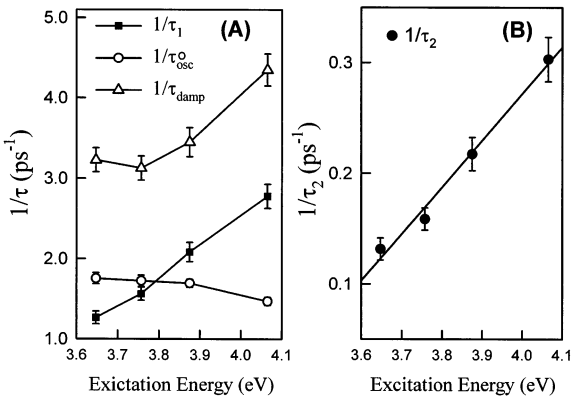

Figure 2. (A) Dependences of $1/\tau_1$, $1/\tau^0_{osc}$, and $1/\tau_{damp}$ on the total excitation energy. (B) Dependence of $1/\tau_2$ on the total excitation energy. The straight line in (B) is a linear fit to the data points and is only meant to guide the eyes.

The transients obtained at all excitation wavelengths can be well fitted to the convolution of a 150 fs fwhm Gaussian instrument response function and a molecular response function composed of a biexponential decay and a damped oscillatory component:

$$M(t) = A_1 \exp(-t/\tau_1) + A_2 \exp(-t/\tau_2) + A_3 \exp(-t/\tau_{damp}) \cos(2\pi t/\tau_{osc}) \quad (1)$$

where τ_1 describes the average signal decay in the first picosecond, τ_2 accounts for the longer decay, τ_{damp} is a damping constant describing the coherence decay, and τ_{osc} is a time-dependent oscillation period defined as $\tau_{osc} = \tau^0_{osc} + at$, where τ^0_{osc} is the initial period and a gives its change with time. This is the simplest model we could find to fit transients at all excitation energies with reasonable qualities. The coefficient a was found to be close to -0.1 for all excitation energies and was therefore fixed at that value in all fits for the sake of consistency. Reciprocals of these time constants are plotted in Figure 2 against the total excitation energy. The initial periods (τ^0_{osc}) correspond to vibrational frequencies of ~50−60 cm^{-1}. Fourier analyses of the transients also revealed broad features centered at similar frequencies.

The biexponential decay component can be understood in view of the asymmetric single-minimum reactive PES.[15,16] Because the largest geometric change occurs along the PT reaction coordinate upon excitation, a major portion of the excess energy (~0.5 eV)[15] is expected to localize in the H-chelate ring region, provided that the initial excitation is much faster than the intramolecular vibrational energy redistribution (IVR). Given the size of the molecule and the amount of excess energy, we expect that IVR should occur rapidly after initial excitation and give rise to the fast decay (τ_1).[20] This vibrational relaxation process removes most of the energy from the O···H···O reaction center and stabilizes the system in the keto configuration. In this sense the initial IVR rate is nearly equivalent to the ESIPT rate, as has been addressed previously.[12] Once stabilized in the keto configuration, the system then decays through some fast nonradiative processes,[12,13] giving rise to the slower exponential decay component (τ_2). These assignments are consistent with the excitation energy dependences of the two rate constants ($1/\tau_1$ and $1/\tau_2$) shown in Figure 2A,B.

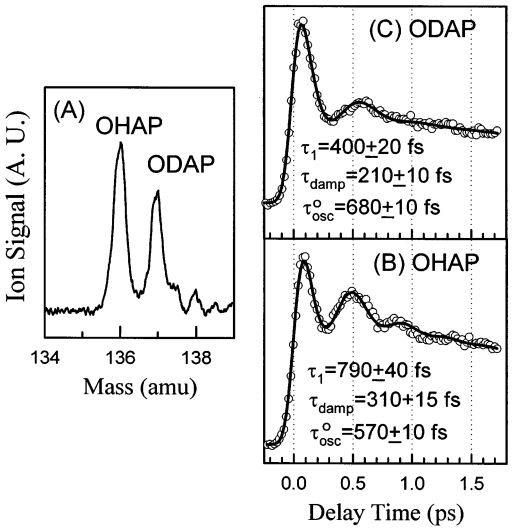

Figure 3. (A) Portion of TOF-MS spectrum showing the mass peaks of OHAP (136 amu) and ODAP (137 amu) obtained with the isotopic mixtures described in the text. (B), (C) Transients obtained by gating the OHAP and ODAP mass peaks shown in (A) under exactly the same conditions. Both transients were obtained with 340 nm excitation. The solid line is the best fit to the model function eq 1 convoluted with the response function. The longer time scale transients (not shown) gave $\tau_2 = 7.6$ ps for OHAP and $\tau_2 = 6.9$ ps for ODAP.

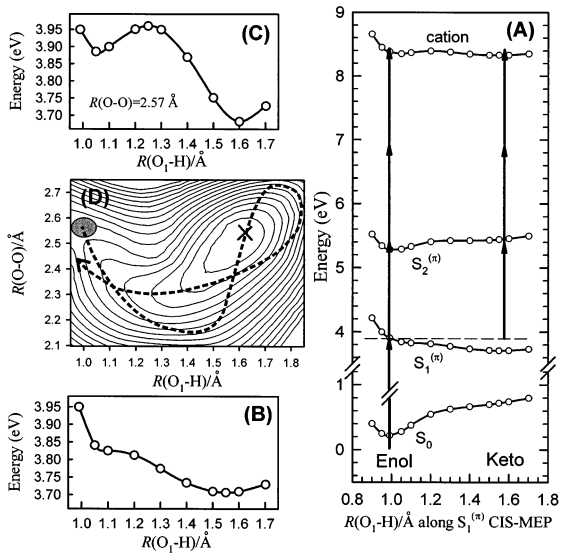

Figure 4. (A) TDDFT PE profile along the $S_1^{(\pi)}$ CIS-MEP for the S_0, $S_1^{(\pi)}$, $S_2^{(\pi)}$, and cationic states of OHAP. Note the variation of the $S_1^{(\pi)}-S_2^{(\pi)}$ energy gap between the enol and keto forms. The solid arrows represent the pump and probe photons. (B) Expanded version of the $S_1^{(\pi)}$ PE curve shown in (A) except that the vertical excitation energy is plotted for the point at the ground-state equilibrium position at $R(O_1-H) = 0.99$ Å. (C) $S_1^{(\pi)}$ TDDFT PE profile along a CIS-optimized path connecting the enol and keto forms with the $R(O-O)$ fixed at 2.57 Å. Note the double-well shape along this path. (D) Schematic $S_1^{(\pi)}$ PE contour map along the O−O and O_1-H coordinates based on the PE profiles shown in (B) and (C). The shaded oval represents the initial wave packet at the Franck−Condon (enol form) region and the cross (×) marks the bottom of the keto well. The dashed line is a possible classical trajectory that oscillates the system between the enol and keto forms.

The most interesting finding of this work is the oscillatory behavior of the transients. This observation implies that there exist some Franck−Condon active modes in the system along which our laser coherent bandwidth (~140 cm^{-1}) is broad enough to create a nuclear wave packet. The wave packet then undergoes a low-frequency vibrational motion that ultimately gives rise to the oscillatory signal. The oscillation frequency increases with time, as indicated by the negative value of the coefficient *a*, and decreases slowly with increasing excitation energy (see Figure 2A). These observations suggest that the wave packet samples a rather anharmonic surface and travels toward narrower regions of the PES while the energy is being relaxed to other modes.

To elucidate the nature of the transient oscillation in relation to the ESIPT reaction, we have also studied the hydroxy-deuterated OHAP (ODAP), in which the H atom of the hydroxy group is replaced with a deuterium atom. A mixture of the two isotopomers was prepared by shaking OHAP liquid with an excess amount of D_2O. The water was then removed from the mixture. The O−H/D isotopic exchange was confirmed by NMR spectroscopy, which showed a consistent OHAP/ODAP ratio with the mass peak ratio observed in the TOF-MS spectrum shown in Figure 3 A. Unambiguous OHAP and ODAP transients, shown in Figure 3B,C, were then obtained by gating the well-separated corresponding mass peaks under exactly the same experimental conditions. The two transients were fitted to the same model function (eq 1), and the results are indicated in Figure 3. In contrast to most previous reports,[12,13] we observed a marked isotope effect. Notably, the IVR rate is increased by almost a factor of 2 and the oscillation period is lengthened by about 100 fs upon hydroxy deuteration. The latter corresponds to a vibrational frequency ratio (ν_H/ν_D) of 1.18. This pronounced isotope effect strongly suggests that *the vibrational motion responsible for the oscillation must involve a substantial displacement of the bridging H atom.* Because no normal modes within the observed low-frequency range in either form of OHAP involve a large enough H-atom motion to account for the large isotope effect,[16,21] we further concluded that the oscillation is not related to any normal mode around any equilibrium configurations of the molecule.

We have also carried out electronic structure theory calculations using the Gaussian 98 program[22] to support our interpretations. Briefly, we calculated the optimized structures of the OHAP first singlet (π,π^*) excited state, hereafter denoted as $S_1^{(\pi)}$,[23] as a function of the distance between the bridging H atom and the phenolic oxygen atom, $R(O_1-H)$,[24] at the CIS level of theory. A basis set based on the 6-31G(d) type with additional diffusion and polarization basis functions added to the two oxygen atoms and the bridging H atom (6-311++G-(d,p)) was used for all calculations presented here. In these calculations, all coordinates were optimized under the planar symmetry constraint whereas $R(O_1-H)$ is fixed at a given value for each point. This gives the $S_1^{(\pi)}$ CIS-optimized minimum-energy path (CIS-MEP) connecting the enol and keto configurations at this level of theory. Single-point energy calculations employing the time-dependent density functional theory (TD-DFT) at the TD-B3LYP level of theory were then carried out for each CIS-optimized structure to obtain the TDDFT potential-energy (PE) profile along the CIS-MEP. This procedure is efficient and has been shown to be at least qualitatively comparable to results obtained at higher levels of theory for molecules of similar sizes.[15] As shown in Figure 4A,B, the TDDFT PE profile for the OHAP $S_1^{(\pi)}$ state along the CIS-MEP is barrierless and has a single minimum corresponding to the keto form. We also calculated the PE profiles for the second singlet (π,π^*) excited state, hereafter denoted as $S_2^{(\pi)}$,[23] at the same level of theory, as well as the neutral and ionic ground states at the B3LYP and UB3LYP levels of theory, respectively, along the $S_1^{(\pi)}$ CIS-MEP. In contrast to the $S_1^{(\pi)}$ state, the $S_2^{(\pi)}$ state has a PE profile similar to that of the S_0 state with a single

minimum corresponding to the enol form, as shown in Figure 4A. This behavior has been pointed out by Nagaoka et al.[25,26] and is consistent with the experimental conclusion that ESIPT does not occur in the $S_2^{(\pi)}$ state of OHAP and OHBA.[25] As a result, the energy gap between the $S_1^{(\pi)}$ and $S_2^{(\pi)}$ states increases from ~1.2 eV near the enol configuration to ~1.7 eV at the $S_1^{(\pi)}$ equilibrium keto configuration. On the other hand, the PE profile of the cationic ground state is predicted to be relatively constant at ~8.35 eV between the two forms. Because the probe photon energy is ~1.5 eV, these results suggest that the MPI probing efficiency may be lower at the keto configuration. This could be simply due to a poorer Franck−Condon overlap for the first probe-photon absorption or a large enough $S_1^{(\pi)}-S_2^{(\pi)}$ energy gap that makes the first probe-photon absorption no longer resonant at the keto configuration. In the latter extreme case the probing has to rely on the much weaker nonresonant absorption, rendering a much smaller ionization cross section near the keto configuration.

Close inspections of these CIS-optimized $S_1^{(\pi)}$ structures revealed that the local geometry of the H-chelate ring undergoes a large change along the CIS-MEP in addition to the lengthening of the O_1-H distance. Most significantly, the distance between the two oxygen atoms, or R(O−O), was found to decrease from 2.57 Å at the initially excited enol configuration to 2.31 Å near the midway along the CIS-MEP and then increase to 2.56 Å again at the keto configuration. Similar theoretical observations have been reported for other ESIPT systems previously.[27−29] On the other hand, the PE profile calculated with the same methodology along a path connecting the enol and keto forms with R(O−O) fixed at 2.57 Å exhibits a double-well shape with a small barrier of ~650 cm^{-1}, as shown in Figure 4C. A qualitative two-dimensional PES, shown in Figure 4D as a contour map, along the O−O and O_1-H coordinates can be inferred on the basis of these results. The most prominent feature of this PES is a barrierless valley along the MEP. At the Franck−Condon region the PE gradient is approximately parallel to the MEP. The initial motion of the wave packet thus involves simultaneous compression of the O−O distance and extension of the O_1-H bond. The shortening in the O−O distance removes the barrier and makes the proton transfer facile. We speculate that this initial motion induces a large-amplitude coherent vibrational motion around the MEP valley. One of the possible classical trajectories is shown in Figure 4D on top of the contour map. This vibrational motion can take the system back to a configuration similar to the enol form and allows the system to oscillate between the two forms. Because the MPI probing cross section is expected to be larger near the enol configuration on the basis of the reasons described above, this coherent vibrational motion modulates the MPI signal of the $S_1^{(\pi)}$ state and gives rise to the observed transient oscillation. The motion described here is consistent with the observed low frequency and large isotope effect, as it incorporates nearly the entire H-chelate ring and involves a substantial displacement of the H atom. While the system oscillates between the two forms, rapid IVR also takes place to remove energy from these two coordinates and finally the trajectory is trapped in the keto well. This partly explains the extremely rapid damping behavior of the oscillation. On the other hand, both the IVR and the large anharmonicity of the reactive PES can cause wave packet dephasing that also contributes to the overall damping.

The combination of experimental and theoretical results given above suggests that the transient oscillation reflects a coherent vibrational motion that follows the molecular transformation from the initial enol configuration to the final keto form during the ESIPT reaction. The observed transients can now be interpreted as follows. Upon initial femtosecond excitation a wave packet is launched on the excited-state surface near the enol configuration. The system then evolves on the excited-state PES with an initial motion involving simultaneous compression of the O−O distance and extension of the O_1-H distance. This initial motion induces a coherent vibrational motion along these two coordinates and oscillates the molecule between the two forms. While the system executes the large-amplitude motion, IVR is also taking place to dissipate energy from the reaction center into other modes and finally stabilizes the system in the keto well. The excited-state keto form then subsequently decays in a longer time scale, i.e., τ_2, through some fast nonradiative processes.[12,13] The oscillation between the two forms modulates the MPI probing efficiency and gives rise to the oscillatory component observed in the transients. This description of ESIPT reaction is not inconsistent with the results of less than 100 fs keto formation time previously reported for similar systems,[12,13] as the initial motion may take less than 100 fs to bring about the keto characteristics and allow the detection of keto formation. The successful detection of the coherent motion here lies in the selectivity of the probing scheme.[1]

Recently, Stock et al.[30] investigated the transient absorption of OHBA in hexane solutions with a time resolution of 30 fs! Oscillatory transients were also observed and were attributed to coherent vibrational motions in three modes in the 140−420 cm^{-1} range. These modes are probably either too high in frequency or too small in amplitude to be observable with our 150 fs time resolution. However, it is interesting to note that the low-frequency motion of ~60 cm^{-1} reported here was not observed in their study. We speculate that the large-amplitude transition-state motion proposed here might be greatly suppressed in solvent cages, manifesting the difference between the gas-phase and condensed-phase reaction dynamics.

IV. Conclusions

We have reported here the first observation of a coherent vibrational motion during the ESIPT reaction under isolated conditions in a molecular beam. The large isotope effect upon hydroxy deuteration and the low frequency (~60 cm^{-1}) led us to conclude that the observed oscillation does not correspond to any normal mode around any equilibrium configurations of the system; instead, it reflects a large-amplitude coherent wave packet motion encompassing both reactant and product regions on the global reactive PES. Theoretical considerations suggested that the motion involves at least two coordinates, O−O and O−H, which are decoupled from the rest of the system for a very short period of time (τ_{damp}) after the initiation of the reaction. The observation of a coherent motion during a reaction in a reduced configuration space[31] in such a complex system implies the feasibility of coherent controls of chemical reactions in large systems.

Acknowledgment. This work was supported by the MOE Program for Promoting Academic Excellence of Universities (89-FA04-AA) and by the National Science Council of the Republic of China (NSC 90-2113-M-007-034).

References and Notes

(1) Zewail, A. H. *Angew. Chem., Int. Ed.* **2000**, *39*, 2586 and references therein.
(2) Rose, T. S.; Rosker, M. J.; Zewail, A. H. *J. Chem. Phys.* **1989**, *91*, 7415.
(3) Gruebele, M.; Zewail, A. H. *J. Chem. Phys.* **1993**, *98*, 883.
(4) Polanyi, J. C.; Zewail, A. H. *Acc. Chem. Res.* **1995**, *28*, 119.

(5) Barbara, P. F.; Walsh, P. K.; Brus, L. E. *J. Phys. Chem.* **1989**, *93*, 29.

(6) Barbara, P. F., Nicol, M., El-Sayed, M. A., Eds. Photoinduced Proton Transfer in Chemistry, Biology and Physics. *J. Phys. Chem.* **1991**, *95*, 10215 and references therein.

(7) Douhal, A.; Lahmani, F.; Zewail, A. H. *Chem. Phys.* **1996**, *207*, 477.

(8) Catalán, J.; Toribio, F.; Acuña, A. U. *J. Phys. Chem.* **1982**, *86*, 303.

(9) Nagaoka, S.; Hirota, N.; Sumitani, M.; Yoshihara, K. *J. Am. Chem. Soc.* **1983**, *105*, 4220.

(10) Nagaoka, S.; Nagashima, U. *Chem. Phys.* **1989**, *136*, 153.

(11) Seliskar, C. J. *J. Mol. Spectrosc.* **1974**, *53*, 140.

(12) Herek, J. L.; Pedersen, S.; Bañares, L.; Zewail, A. H. *J. Chem. Phys.* **1992**, *97*, 9046.

(13) Lochbrunner, S.; Schultz, T.; Schmitt, M.; Shaffer, J. P.; Zgierski, M. Z.; Stolow, A. *J. Chem. Phys.* **2001**, *114*, 2519.

(14) Sobolewski, A. L.; Domcke, W. *Chem. Phys.* **1994**, *184*, 115.

(15) Sobolewski, A. L.; Domcke, W. *Phys. Chem. Chem. Phys.* **1999**, *1*, 3065.

(16) Vener, M. V.; Scheiner, S. *J. Phys. Chem.* **1995**, *99*, 642.

(17) Chudoba, C.; Riedle, E.; Pfeiffer, M.; Elsaesser, T. *Chem. Phys. Lett.* **1996**, *263*, 622.

(18) Lochbrunner, S.; Wurzer, A. J.; Riedle, E. *J. Chem. Phys.* **2000**, *112*, 10699.

(19) Scherer, N. F.; Khundkar, L. R.; Rose, T. S.; Zewail, A. H. *J. Phys. Chem.* **1987**, *91*, 6478.

(20) Felker, P. M.; Zewail, A. H. Ultrafast Dynamics of IVR in Molecules and Reactions. In *Jet Spectroscopy and Molecular Dynamics*; Hollas, M., Phillips, D., Eds.; Blackie Academics and Professional: Glasgow, 1995.

(21) For example, our excited-state vibrational frequency calculations at the CIS level gave a few low-frequency modes below 250 cm^{-1}, including the CH_3 torsional, CH_3 wagging, and skeleton out-of-plane bending modes. Nonetheless, these modes cannot be responsible for the coherent vibration observed here because they do not involve a large displacement in the bridging H atom and therefore cannot account for the observed large isotope effect. In fact, the calculated isotope vibratioanl frequency ratios (ν_H/ν_D) are in the 1.003−1.007 range for these modes, much smaller than the observed value of 1.18.

(22) Frisch, M. J.; Trucks, G. W.; Schlegel, H. B.; Scuseria, G. E.; Robb, M. A.; Cheeseman, J. R.; Zakrzewski, V. G.; Montgomery, J. A., Jr.; Stratmann, R. E.; Burant, J. C.; Dapprich, S.; Millam, J. M.; Daniels, A. D.; Kudin, K. N.; Strain, M. C.; Farkas, O.; Tomasi, J.; Barone, V.; Cossi, M.; Cammi, R.; Mennucci, B.; Pomelli, C.; Adamo, C.; Clifford, S.; Ochterski, J.; Petersson, G. A.; Ayala, P. Y.; Cui, Q.; Morokuma, K.; Malick, D. K.; Rabuck, A. D.; Raghavachari, K.; Foresman, J. B.; Cioslowski, J.; Ortiz, J. V.; Stefanov, B. B.; Liu, G.; Liashenko, A.; Piskorz, P.; Komaromi, I.; Gomperts, R.; Martin, R. L.; Fox, D. J.; Keith, T.; Al-Laham, M. A.; Peng, C. Y.; Nanayakkara, A.; Gonzalez, C.; Challacombe, M.; Gill, P. M. W.; Johnson, B. G.; Chen, W.; Wong, M. W.; Andres, J. L.; Head-Gordon, M.; Replogle, E. S.; Pople, J. A. *Gaussian 98*, revision A.9; Gaussian, Inc.: Pittsburgh, PA, 1998.

(23) Because the first $^1(n,\pi^*)$ state is nearly degenerate to the first $^1(\pi,\pi^*)$ state around the enol configuration and their exact ordering is not known, here we followed the notations used in ref 9; i.e., $S_1^{(\pi)}$ denotes the first singlet (π,π^*) state and $S_2^{(\pi)}$ the second singlet (π,π^*) state, to avoid confusion.

(24) O_1 denotes the oxygen atom to which the hydrogen atom is covalently bonded in the ground-state enol form, whereas O_2 denotes the other oxygen atom.

(25) Nagaoka, S.; Nagashima, U.; Ohta, N.; Fujita, M.; Takemura, T. *J. Phys. Chem.* **1988**, *92*, 166.

(26) Nagaoka, S.; Shinde, Y.; Mukai, K.; Nagashima, U. *J. Phys. Chem. A* **1997**, *101*, 3061.

(27) Bell, R. L.; Truong, T. N. *J. Chem. Phys.* **1994**, *101*, 10442.

(28) Guallar, V.; Moreno, M.; Lluch, J. M.; Amat-Guerri, F.; Douhal, A. *J. Phys. Chem.* **1996**, *100*, 19789.

(29) Organero, J. A.; Moreno, M.; Santos, L.; Lluch, J. M., Douhal, A. *J. Phys. Chem. A* **2000**, *104*, 8424.

(30) Stock, K.; Bizjak, T.; Lochbrunner, S. *Chem. Phys. Lett.* **2002**, *354*, 409.

(31) Kotting, C.; Diau, E. W.-G.; Baldwin, J. E.; Zewail, A. H. *J. Phys. Chem.* **2001**, *105*, 1677.